Available online at www.sciencedirect.com
SCIENCE DIRECT®
Thermochimica Acta 432 (2005) 23–29
thermochimica acta
www.elsevier.com/locate/tca

Solid–liquid equilibrium diagrams of common ion binary salt hydrate mixtures involving nitrates and chlorides of magnesium, cobalt, nickel, manganese, and iron(III)

Y. Marcus *, A. Minevich, L. Ben-Dor

Department of Inorganic and Analytical Chemistry, The Hebrew University, Jerusalem 91904, Israel

Received 20 December 2004; received in revised form 3 April 2005; accepted 7 April 2005
Available online 3 May 2005

Abstract

The solid–liquid equilibrium diagrams of binary mixtures involving magnesium nitrate hexahydrate with cobalt nitrate hexahydrate, nickel nitrate hexahydrate (partly), manganese nitrate tetrahydrate, and iron(III) nitrate nonahydrate and of magnesium chloride hexahydrate with cobalt and nickel chlorides hexahydrates and manganese chloride tetrahydrate, and the of two manganese salts were determined. Those diagrams that showed a simple eutectic were fitted by the Ott equation and where the required BET parameters were available, the magnesium salt rich parts of the liquidus were modeled by means of this method.

Keywords: BET modeling; Metal chlorides; Metal nitrates; Phase diagram; Salt hydrates

1. Introduction

Solid–liquid phase diagrams of binary mixtures of salts abound in the literature, but equilibrium diagrams of binary mixtures of salt hydrates have so far been published in few cases only. The complete diagrams over the entire composition range were reported many years ago by Mokhosoev and Got'manova [1] for several divalent metal nitrates and by Marcus et al. [2] for magnesium chloride and bromide hexahydrates. The present authors have recently reported the complete phase diagrams for the hydrates of magnesium nitrate and acetate, and magnesium and aluminum nitrates [3], and of mixtures of ammonium alum with ammonium sulfate and aluminum sulfate [3] and with ammonium nitrate, aluminum nitrate, and ammonium iron(III) alum as well as of aluminum nitrate with aluminum sulfate [4]. Zeng and Voigt [5] reported isothermal ternary phase diagrams including cuts for binary salt hydrate mixtures of lithium nitrate with magnesium and calcium nitrates and with lithium perchlorate, for which some experimental data near ambient temperatures were available. No liquidus curves of these systems were, however shown. Of course, many publications have dealt with salt hydrates, including mixtures, in the presence of excess water, for example the recent report by Ibnlfassi et al. [6], but these are not really relevant to the present subject.

In the present paper, we report the solid–liquid equilibrium diagrams of binary mixtures of magnesium nitrate hexahydrate with cobalt, nickel (partly), manganese, and iron(III) nitrate hydrates and of magnesium chloride hexahydrate with cobalt, nickel, and manganese chloride hydrates, and of the two manganese salt tetrahydrates. Some of these diagrams exhibit a single eutectic whereas others have indications of the formation of a congruently melting compound at a certain composition.

The solid–liquid phase diagrams of binary systems A + B that exhibit a sharp minimum (a eutectic) can be fitted with the semi-empirical Ott equation [7]:

$$T(x) = T^*[1 + \Sigma a_i(x - x^*)^i] \quad (1)$$

where $x = x_B$. In the A-rich side $T^* = T_m(A)$, the melting point of component A, and $x^* = 1$ with one set of a_i parame-

* Corresponding author. Tel.: +972 2 6585341; fax: +972 2 6585319.
E-mail address: ymarcus@vms.huji.ac.il (Y. Marcus).

0040-6031/$ – see front matter © 2005 Elsevier B.V. All rights reserved.
doi:10.1016/j.tca.2005.04.003

ters and for the B-rich side, beyond the eutectic, $T^* = T_m(B)$ and $x^* = 0$ with a second set of a_i parameters. These parameters, however, have no relationship to the properties of the individual salts A and B.

In certain cases, where the required information for the individual salt hydrates is available, the liquidus can be modeled by means of the BET method. The needed data are the BET parameters r, the number of sites per formula unit of the salt, and ε, the excess condensation energy of water vapor on the salt for the two components A and B, as well as the molar freezing enthalpy of that component that crystallizes out of the melt. This was done very recently for some cases by Zeng and Voigt [3], by Marcus et al. [4], and by Marcus [8]. The operative expression for this purpose pertaining to the salt A crystallizing from the mixture is [8]:

$$\ln[a_A(T, x_A)a_W^{j_A}(T, x_A)] = Q\left[\frac{1}{T} - \frac{1}{T_{mA}}\right] + D \quad (2)$$

where a_A and a_W are the activities of the salt A and water W, calculated from the BET parameters r and ε, x_A is the fraction of A in the binary A + B mixture, T_{mA} is the melting point of pure A, and j_A is the hydrate number of A. The quantity RQ represents the enthalpy of crystallization of A corrected for the excess enthalpies of the salt and water that constitute roughly 10% of it. The function Q, thus is:

$$Q = \frac{(L_A - H_A^E - j_A H_W^E)}{R} \quad (3)$$

where L_A is the molar enthalpy of melting, H^E is the partial molar excess enthalpy in the melt of salt A and of water W. The function D is $(1/RT)$ times the chemical potential of A in the melt at equilibrium with the crystalline salt hydrate for pure A (at $x_A = 1$) at its melting point T_{mA}:

$$D = \ln[a_A(T_{mA}, 1)a_W^{j_A}(T_{mA}, 1)] \quad (4)$$

The procedure followed by the computation program is to vary the temperature T from T_m downwards at a given fraction x_A until the two sides of Eq. (2) become equal within a preset limit, and that value of T is the liquidus point for this composition. For further details see Ref. [8].

2. Experimental

2.1. Materials

Magnesium nitrate hexahydrate (Baker's Analyzed), $Mg(NO_3)_2{\cdot}6H_2O$, abbreviated **MgN**, water content 6.02 ± 0.01 mol of water per mol salt, determined by EDTA and by Karl-Fischer titrations. Iron(III) nitrate nonahydrate $Fe(NO_3)_3{\cdot}9H_2O$ (Fluka), abbreviated **FeN**, nickel nitrate hexahydrate $Ni(NO_3)_2{\cdot}6H_2O$ (Arcos), abbreviated **NiN**, cobalt nitrate hexahydrate $Co(NO_3)_2{\cdot}6H_2O$ (Riedel de Haën), abbreviated **CoN**, and manganese nitrate tetrahydrate $Mn(NO_3)_2{\cdot}4H_2O$ (Merck), abbreviated **MnN**, were the best available analytical reagents and were used as received. The water contents of the hydrated salts **FeN** and **NiN** were measured by titration of the metal ions and no appreciable deviations from the nominal contents were noted. Magnesium chloride hexahydrate (Gadot), $MgCl_2{\cdot}6H_2O$, abbreviated **MgC**, nickel chloride hexahydrate $NiCl_2{\cdot}6H_2O$ (BDH), abbreviated **NiC**, cobalt chloride hexahydrate $CoCl_2{\cdot}6H_2O$ (Matheson, Coleman, and Bell), abbreviated **CoC**, and manganese chloride tetrahydrate $MnCl_2{\cdot}4H_2O$ (Baker's Analyzed and Merck), abbreviated **MnC**, were also the best available analytical reagents and were used as received. Well crystallized kaolinite $Al_4Si_4O_{10}(OH)_8$ from Washington County, GA, abbreviated Ka, was used as a nucleating and thickening agent.

2.2. X-ray characterization

A Philips Automatic Powder Diffractometer was employed, with monochromatized Cu Kα radiation. Crystals of $Mg(NO_3)_2{\cdot}6H_2O$ (**MgN**), $Ni(NO_3)_2{\cdot}6H_2O$ (**NiN**), and $Co(NO_3)_2{\cdot}6H_2O$ (**CoN**) were ground finely, and their powder diffractions were measured. The diffraction patterns agreed with those in the literature [9–11] (2000 JCPDS). Crystals of $MnCl_2{\cdot}4H_2O$ (**MnC**) and of $Mn(NO_3)_2{\cdot}4H_2O$ (**MnN**) were also ground finely and their powder diffractions were measured. Their diffractograms agreed with those in the literature [12,13] (2002 JCPDS).

2.3. Phase diagrams of mixtures

These were obtained for mixtures prepared on a mole fraction basis in the manner reported previously [3–5], i.e., by following cooling curves (temperature versus time) and visually. An example of such cooling curves, for pure $Ni(NO_3)_2{\cdot}6H_2O$, is shown in Fig. 1. Three cycles of melting and cooling in an open test-tube, with 1% kaolinite as

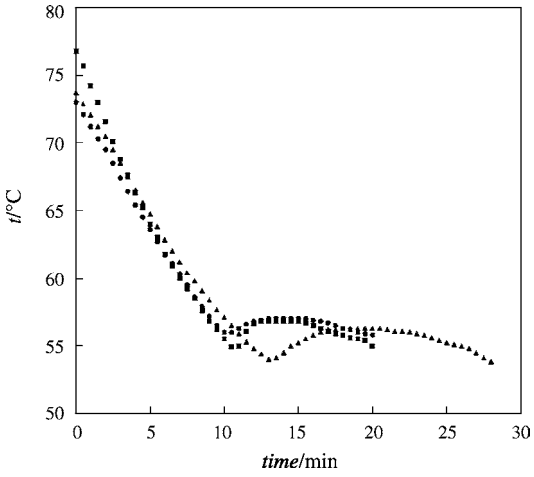

Fig. 1. Cooling curves of $Ni(NO_3)_2{\cdot}6H_2O$ for two consecutive cycles of one sample, '●' (t_m = 57.0 °C) and '▲' (t_m = 56.3 °C), and for a different sample, '■' (t_m = 56.8 °C).

nucleating and thickening agent, were generally employed and the freezing temperatures reported are the means of the temperature halts noted in these curves, generally reproducible to ±1 °C unless otherwise noted in the results. When the freezing point of the melt was low, around or below ambient temperatures, the viscosity was fairly high, and in the case of eutectics the expected second halt in the cooling curves could not then be observed.

3. Results

3.1. Individual salts

The measured freezing temperatures of the individual salt hydrates are reported in Table 1. All the salts were melted and frozen reversibly and reproducibly, including the yellow crystals of **FeN**, melting to a clear brown liquid. Molten **CoC** appears to be a solution of a mixture of the hexa- and di-hydrates in the water of crystallization. The transition temperature between the two solid salts obtained [16] from the vapor pressures is $t_{tr} = 52.25$ °C, but in the present study it was found that the hexahydrate crystallized out. Molten **NiC** appears to be a solution of a mixture of the hexa- and tetrahydrates in the water of crystallization. The transition temperature between the two solid salts obtained from the vapor pressures [16] is $t_{tr} = 36.25$ °C. In our experiments, the hexahydrate crystallized out from the melt at its freezing point. **MnC** melted and froze reproducibly at 50 ± 1 °C, below the transition point to the dihydrate at 58 °C, reported as its melting point [14].

3.2. X-ray characterization

Equimolar crystalline mixtures of magnesium nitrate (**MgN**) with nickel nitrate (**NiN**) and with cobalt nitrate (**CoN**) obtained either from the melt or grown from aqueous solutions showed the same powder diffraction patterns [18], identical with that of pure **CoN**. In the diffractogram of crystals grown from an aqueous solution or from the melt of an equimolar mixture of **MgN** + **MnN** new diffraction lines were found that did not belong to the components, signifying a new compound that was formed.

Table 1
The freezing temperatures of the salt hydrates

Salt	T_m (°C) this study	T_m (°C) literature
$Mg(NO_3)_2{\cdot}6H_2O$, **MgN**	89.5 ± 0.5	89.5 [4]
$Co(NO_3)_2{\cdot}6H_2O$, **CoN**	51.5 ± 0.5	55.5 [14]
$Ni(NO_3)_2{\cdot}6H_2O$, **NiN**	56.7 ± 0.5	56.7 [14]
$Fe(NO_3)_3{\cdot}9H_2O$, **FeN**	43.3 ± 2.0	48.7 [14]
$Mn(NO_3)_2{\cdot}4H_2O$, **MnN**	33.1 ± 0.5	37.1 [15]
$MgCl_2{\cdot}6H_2O$, **MgC**	112.0 ± 1.0	116.2 [2], 117 [14]
$CoCl_2{\cdot}6H_2O$, **CoC**	47.3 ± 0.5	52.25 [16]
$NiCl_2{\cdot}6H_2O$, **NiC**	30.2 ± 0.5	36.25 [16], 60 [17]
$MnCl_2{\cdot}4H_2O$, **MnC**	50.0 ± 1.0	58 [14]

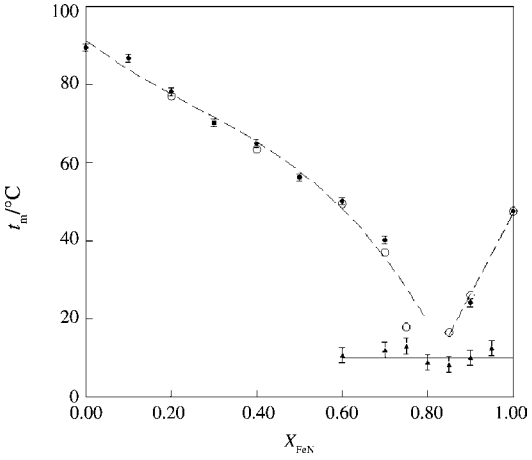

Fig. 2. The liquidus of the phase diagram of **MgN** + **FeN**. The freezing point is t_m in °C; '●' first series of experiments, '◯' second series of experiments, '▲' second break in the cooling curve, signifying the eutectic temperature; '---' fitting by Eq. (1) with the parameters from Table 2.

3.3. Solid–liquid equilibrium diagrams

The solid–liquid equilibrium diagrams of the salts determined in this work are shown in Figs. 2–9. Eq. (1) was used for fitting the phase diagram empirically by the Ott expression, with the resulting parameters shown in Table 2. The results of this fitting are also shown in Figs. 2–9.

In the solid–liquid equilibrium diagram of the **MgN** + **FeN** system, Fig. 2, a eutectic is observed near $x_{FeN} = 0.8$ with $t_m = 10.8 \pm 2.0$ °C. The exact composition could not be determined since the melts were rather viscous at this low temperature. In spite of the tendency of iron(III) salts to hydrolyze, the melting and freezing of this salt itself and in the mixtures were reversible.

The solid–liquid equilibrium diagram of **MgN** + **CoN** mixtures, Fig. 3, shows a reproducible break in the continuous decreasing $t_m(x_{CoN})$ curve in the $0.30 \leq x_{CoN} \leq 0.35$ region.

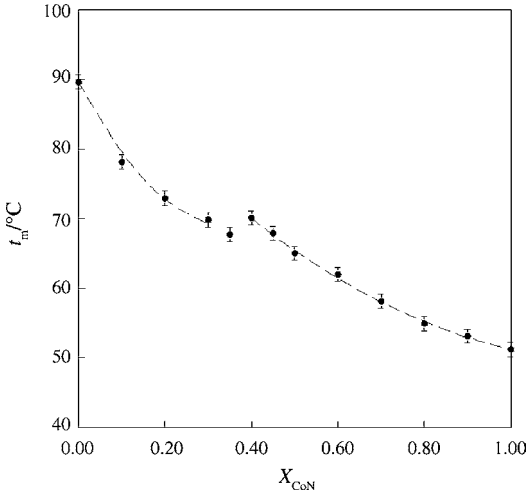

Fig. 3. The liquidus of the phase diagram of **MgN** + **CoN**. The freezing point '●' is t_m in °C; '---' fitting by Eq. (1) with parameters from Table 2.

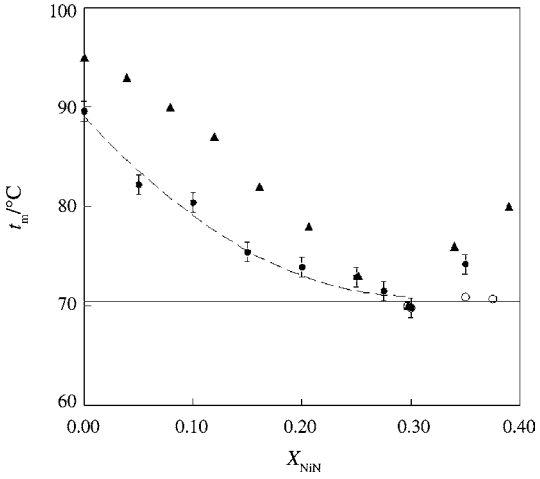

Fig. 4. The liquidus of a partial phase diagram of **MgN** + **NiN**. The freezing point '●' is t_m in °C; '- - -' fitting by Eq. (1) with parameters from Table 2; the second halt signifying the eutectic is O; and '▲' are data from [1].

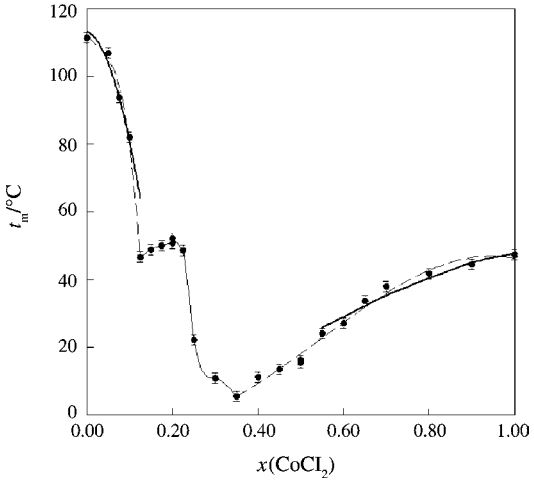

Fig. 6. The liquidus of the phase diagram of **MgC** + **CoC**. The freezing point '●' is t_m in °C; '- - -' fitting by Eq. (1) with parameters from Table 2. The thin continuous curve was passed between the data points not included in the fitting, $0.18 \leq x_{CoC} \leq 0.35$. '—' modeling by the BET method, Eqs. (2)–(4).

However, the X-ray diffraction results did not show the formation of a new crystalline phase at that or the equimolar composition, so that the origin of the small maximum in the curve at $x_{CoN} = 0.40$ is obscure, as is the reality of a eutectic at $x_{CoN} = 0.30$. Still, two separate branches of the Ott fitting curves are obtained for the purpose of fitting the data. If the break in the curve is disregarded, then this diagram indicates complete solid solution formation in the crystals, as indicated also by the ready distribution of magnesium ions in the cobalt nitrate hydrate crystal lattice [18].

The solid–liquid equilibrium diagram of **MgN** + **NiN**, having been already published [1], has not been studied again fully. Since, however, the reported [1] t_m of **MgN** was as high as 95 °C rather than the accepted 89.5 °C, the region of the diagram diluted in **NiN** was re-determined, as shown in Fig. 3. The existence of the eutectic at $x_{NiN} = 0.30$, $t_m = 70.4 \pm 0.5$ °C, was confirmed. The formation of a congruently melting compound at $x_{NiN} = 0.50$ [1] was also confirmed and its structure, determined by single crystal X-ray diffraction, is reported elsewhere [18]. The **MgN**-rich part of the liquidus curve has already been modeled successfully by the BET method [8].

The solid-liquid equilibrium diagram of **MgN** + **MnN** mixtures is shown in Fig. 5 and appears to be of a simple eutectic type, with a shallow minimum with $t_m = 26.2$ °C at $0.7 \leq x_{MnN} \leq 0.9$. However, no second halt in the cooling curves was observed, so that the eutectic could not be characterized more definitely. The Ott fitting parameters for the **MgN**-rich branch is shown in Table 1. This system could be modeled by the BET method, Eqs. (2)–(4), as seen in Fig. 4, since the required r and ε BET parameters were available [8].

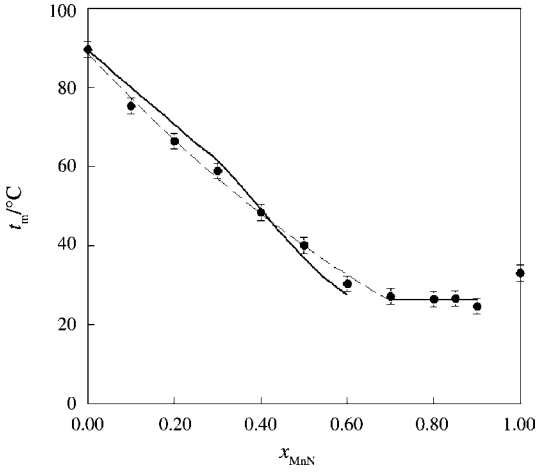

Fig. 5. The liquidus of the phase diagram of **MgN** + **MnN**. The freezing point '●' is t_m in °C; '- - -' fitting by Eq. (1) with parameters from Table 2; '—' modeling by the BET method, Eqs. (2)–(4).

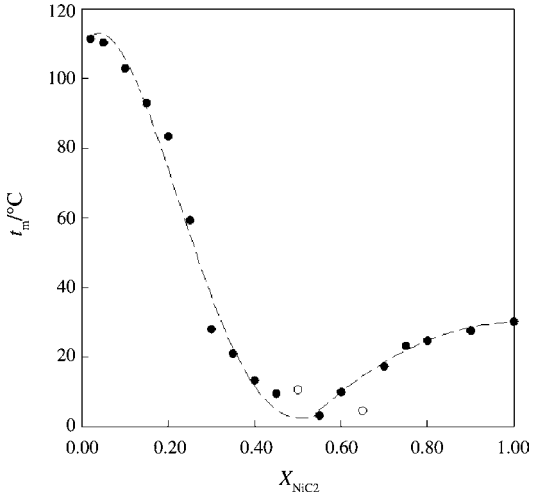

Fig. 7. The liquidus of the phase diagram of **MgC** + **NiC**. The freezing point '●' is t_m in °C; '- - -' fitting by Eq. (1) with parameters from Table 2. (The data marked by O were not included in the fitting.).

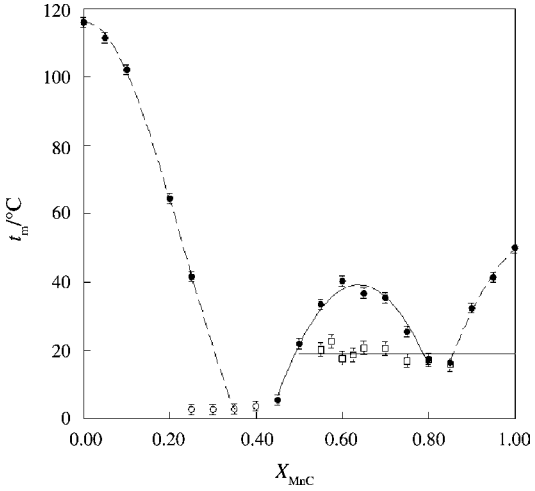

Fig. 8. The liquidus of the phase diagram of **MgC** + **MnC**. The freezing point '●' is t_m in °C; 'O' and '□' denote the halts in the cooling curve for the eutectics. The dashed curves '---' shows the fitting by Eq. (1) with parameters from Table 2, the continuous curve is drawn as an eye guide only.

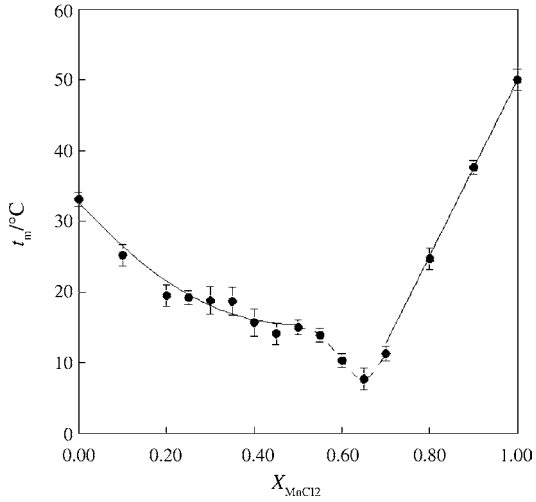

Fig. 9. The liquidus of the phase diagram of **MnN** + **MnC**. The freezing point '●' is t_m in °C; '—' fitting by Eq. (1) with parameters from Table 2, '---' part of the diagram that is not fitted.

The solid–liquid equilibrium diagram of **MgC** + **CoC** mixtures shown in Fig. 6 has a shallow eutectic with $t_m = 46.6 \pm 0.8$ °C at $x_{CoC} = 0.13$ followed by a maximum $t_m = 52.1 \pm 0.8$ °C at $x_{CoC} = 0.20$. This is then followed by a eutectic with the minimal $t_m = 5.2 \pm 0.8$ °C at $x_{CoC} = 0.35$. However, no second halt in the cooling curves was observed, so that the eutectic could not be characterized more definitely. In this system, too, both branches of the liquidus could be modeled by the BET method to a fairly long extent towards the eutectics formed, see Fig. 6.

The solid–liquid equilibrium diagram of **MgC** + **NiC** mixtures shown in Fig. 7 is of a simple eutectic type, with a rather broad minimal $t_m = 3.5 \pm 0.8$ °C at $x_{NiC} \approx 0.55$. However, as for the **MgC** + **CoC** mixtures, no second halt in the cooling curves was observed, so that the eutectic could not be characterized more definitely. The **MgC**-rich part of the liquidus curve has already been modeled successfully by the BET method [8].

The solid–liquid equilibrium diagram of **MgC** + **MnC** mixtures is shown in Fig. 8. It is characterized by two eutectics, at ∼2 °C and $x_{MnC} \sim 0.4$ and at ∼17 °C and $x_{MnC} \sim 0.8$, and an apparently congruently melting compound, with $t_m \sim 41$ °C at $x_{MnC} \sim 0.65$, i.e, 2 $MnCl_2$: 1 $MgCl_2$. The first eutectic may be at an even lower temperature than 2 °C, since complete freezing could not be observed in the cooling curves. However, this feature was reproducible over several cycles.

Finally, the solid–liquid equilibrium diagram of **MnN** + **MnC** mixtures is shown in Fig. 9. It has a clear eutectic at $x_{MnC} = 0.65$ and 7.7 ± 1.0 °C, but possibly some features at x_{MnC} ∼0.3 and ∼0.5 may indicate compound formation, although the data at $0.3 \leq x_{MnC} \leq 0.45$ were not

Table 2
Parameters of the Ott Eq. (1)

System	*x*-Range	*T**	a_0	a_1	a_2	a_3
(1–*x*)**MgN** + *x***FeN**	0.00–0.75	89.5	−0.85	−1.09	−0.23	
(1–*x*)**MgN** + *x***FeN**	0.85–1.00	47.5	−4.38	4.37		
(1–*x*)**MgN** + *x***CoN**	0.00–0.35	89.5	0.51	2.32	1.81	
(1–*x*)**MgN** + *x***CoN**	0.45–1.00	51.2	0.83	−1.38	0.55	
(1–*x*)**MgN** + *x***NiN**	0.00–0.30	89.5	0.87	3.09	2.21	
(1–*x*)**MgN** + *x***MnN**	0.00–0.70	89.5	−0.85	−0.297	0.653	0.107
(1–*x*)**MgC** + *x***CoC**	0.00–0.18	112[a]	−428.99	−1318.00	−1350.75	−461.74
(1–*x*)**MgC** + *x***CoC**	0.35–1.00	47.3	−0.952	−1.616	6.602	−4.057
(1–*x*)**MgC** + *x***NiC**	0.00–0.55	112[a]	−2.83	−18.47	−60.22	−78.20[b]
(1–*x*)**MgC** + *x***NiC**	0.55–1.00	30.2	−4.04	7.99	−3.95	
(1–*x*)**MgC** + *x***MnC**	0.00–0.35	116.0	3.3	23.9	37.6	17.1
(1–*x*)**MgC** + *x***MnC**	0.80–1.00	50.0	−17.0	31.8	−14.8	
(1–*x*)**MnN** + *x***MnC**	0.00–0.50	33.1	0.0	2.12	2.105	
(1–*x*)**MnN** + *x***MnC**	0.70–1.00	50.0	−2.48	2.48		

[a] A value that is ∼4 to 5 °C lower than the accepted value.
[b] A further term is required with $a_4 = -33.65$.

as well reproducible in the three cycles as outside this region.

4. Discussion

The freezing points $t_m = t_{freeze}$ of the molten salt hydrates and their mixtures provide the liquidus of the solid–liquid equilibrium diagram. Those of the pure components, Table 1, are sometimes lower than the melting temperatures t_{melt} recorded in the literature. One reason for this discrepancy is that the published t_{melt} is commonly the temperature of the endothermic peak in a DSC determination that may lag behind the actual start of the melting of the sample. Another reason for the discrepancy may be small differences in the water contents of the salt hydrate. In the present study, the nominal water contents of the crystalline salt hydrates was confirmed within 0.05 mol water per mole salt, and a differing water content should not be a reason for incorrect values of the measured $t_m = t_{freeze}$. Furthermore, the presence of the kaolinite as a nucleating and thickening agent caused the undercooling of the melt before freezing, if at all, not to exceed 2 °C, see for example Fig. 1. A clear halt in the cooling curve (temperature against time) resulted after the temperature rose to the equilibrium value.

Several interesting features were found in the phase diagrams determined in this study. In two cases, the **MgN** + **FeN** and **MgN** + **MnN** systems, Figs. 2 and 5, there seems to be a single eutectic at the **FeN**, respectively **MnN**-rich part of the diagram. The mixture **MgC** + **NiC** Fig. 7, may also be of this type, although the eutectic halt near the equimolar composition (a second halt in the cooling curve) was not seen. This system shares with the **MgC** + **MnC** system, Fig. 8, the continued existence of the liquid molten salt hydrate mixture to very low temperatures near the freezing point of water and a very steep decline of t_m from that of **MgC** with increasing contents of the co-salt. A clear indication of the formation of a congruently melting compound is seen in the cases of **MgC** + **CoC** and **MgC** + **MnC**, Figs. 6 and 8. Attempts to characterize the compounds by X-ray diffraction have so far not been successful since no single crystals have grown from saturated aqueous solutions of suitable compositions. On the other hand, powder X-ray diffraction of an equimolar mixture of **MgN** + **MnN** did indicate that a new compound was present, although the phase diagram did not show a corresponding feature. The phase diagram of **MgN** + **NiN** system was studied many years ago [1]. However, since the **MgN** in that publication was said to have a melting point of 95 °C, considerably higher than the accepted value of 89.5 °C [3], the melting points of the mixtures reported previously [1] and shown in Fig. 4 cannot be correct. Still, the eutectic temperature reported previously was now confirmed and the system did show that a congruently melting compound was formed, as previously reported, and its single crystal X-ray diffraction [18] showed its structure to correspond to that of **CoN** [11]. Finally, the **MgN** + **CoN** and **MnN** + **MnC** systems, Figs. 3 and 9, have some indication of a compound being formed but not as well defined maxima in the phase diagram between two eutectics, as e.g., in the **MgN** + **NiN** [1] and **MgC** + **MnC** (Fig. 8) mixtures. The features in the **MgN** + **CoN** and **MnN** + **MnC** systems may, after all, be artifacts as no new phases could be detected by X-ray diffraction.

The modeling of at least some parts of the liquidus curves by means of the BET method indicates that the assumptions on which the method is based have some validity. Apart from the formal description of the salt hydrate melts as if the water is adsorbed on sites of the salt (disregarding its ionic dissociation), there is the assumption concerning mixing rules of the parameters r and ε in the binary melt. These rules are: $r = x_A r_A + x_B r_B$ and $\varepsilon = (x_A r_A \varepsilon_A + x_B r_B \varepsilon_B)/r$, so that a central assumption for the modeling of the mixtures is that they behave ideally, as discussed previously [8]. The chemical potential of the component A in the binary melt of A + B, given by the left hand side of Eq. (2) and calculated by means of these mixing rules, is crucial for modeling the liquidus. The successful modeling indicates that the excess entropy of mixing is small. The excess enthalpies are taken into account in Eq. (3), and appear not to be large either, lending support to the assumption of near ideal mixing in the melt.

5. Conclusions

The meager information in the literature concerning the solid–liquid equilibrium diagrams of binary mixtures of salt hydrates is augmented here with liquidus diagrams for seven systems over the entire composition range. These comprise mixtures of magnesium nitrate hexahydrate (**MgN**) with cobalt nitrate hexahydrate (**CoN**), with iron(III) nitrate nonahydrate (**FeN**), and with manganese nitrate tetrahydrate (**MnN**), and of magnesium chloride hexahydrate (**MgC**) with cobalt chloride hexahydrate (**CoC**), with nickel chloride hexahydrate (**NiC**), and with manganese chloride tetrahydrate (**MnC**), as well as of the two manganese salts. The magnesium nitrate rich part of the diagram with nickel nitrate (both hexahydrates) was re-determined. Three of these systems (**MgN** + **FeN**, **MgN** + **MnN**, and **MgC** + **NiC**) have single eutectics as their only clear features and one (**MgN** + **MnC**) may have a peritectic, in addition to a eutectic. One system, the **MgN** + **CoN** one, does not appear to have a well characterized eutectic. Three systems (**MgN** + **NiN**, **MgC** + **CoC**, and **MgC** + **MnC**) show maximal melting temperatures signifying compound formation and the two eutectics around it (in the case of **MgN** + **NiN** only the **MgN**-rich branche is shown). Some of the eutectics have very low freezing points, <10 °C, the melts being then fairly viscous, so that only the minima in the liquidus curves could be reported. In some of the systems a considerable part of the liquidus of the magnesium salt rich part of the diagram could be modeled by means of the BET method. Where this could not be done this was due to the BET parameters, r and ε, not being available either for

the non-magnesium component (e.g., **MgN** + **FeN**) or for the congruently melting compounds (e.g., **MgC** + **MnC**).

Acknowledgement

The research was supported by a grant from the German Federal Ministry for the Environment, Nature Coservation, and Nuclear Safety and the Israeli Ministry of Science and Technology, within the German-Israeli Energy Research program.

References

[1] M.V. Mokhosoev, T.T. Got'manova, Russ. J. Inorg. Chem. 11 (1966) 466–469.
[2] Y. Marcus, V. Dangor, S. Lessery, Thermochim. Acta 77 (1984) 216–226.
[3] Y. Marcus, A. Minevich, L. Ben-Dor, Thermochim. Acta 412 (2004) 163–170.
[4] Y. Marcus, A. Minevich, L. Ben-Dor, J. Therm. Anal. Calorim, in press.
[5] D. Zeng, W. Voigt, Comput. Coupl. Phase Diagrams Thermochem. 27 (2003) 243–251.
[6] A. Ibnlfassi, M. Kaddami, K. El Kacemi, J. Therm. Anal. Calorim. 74 (2003) 341.
[7] J.B. Ott, J.R. Goates, J. Chem. Thermodyn. 15 (1983) 267–278.
[8] Y. Marcus, J. Solution Chem., in press.
[9] MgN: A. Braibanti, A. Tiripicchio, A.M. Manotti-Lanfredi, F. Bigoli, Acta Cryst. E, 25 (1969) 354–361; International Center for Diffraction Data, 2000, card no. 14-0101: monoclinic, P21/c.
[10] NiN: Natl. Bureau Stand. (U.S.) (1974). Monograph 25, 12, 26; International Center for Diffraction Data, 2000, card no. 25-0577: triclinic.
[11] CoN: P.V. Prelesnik, F. Gabela, B. Ribar, I. Krstanovic, Cryst. Struc. Comm. 2, 581–583 (1973); International Center for Diffraction Data, 2000, card no. 9263: monoclinic, C1 2/c1.
[12] MnC: Natl. Bureau Stand. (U.S.) Monograph 25, 9, 28 (1971); International Center for Diffraction Data, 2002, card no. 22-0721: monoclinic, P21/n.
[13] MnN: D. Popov, R. Herak, B. Prelesni, B. Ribar, Z. Kristallorg, 137, (1973) 280–289.
[14] J. Guion, D.D. Sauzade, M. Laügt, Thermochim. Acta 67 (1983) 167–179.
[15] W.W. Ewing, H.E. Rasmussen, J. Am. Chem. Soc. 64 (1942) 1443–1445.
[16] I.H. Derby, V. Yngve, J. Am. Chem. Soc. 38 (1916) 1439–1452.
[17] W.W. Wendlandt, Thermochim. Acta 9 (1974) 101–107.
[18] S. Cohen, G. Wollmann, L. Ben-Dor, Y. Marcus, J. Cryst. Growth 270 (2004) 589–592.